Article

Cell Chemical Biology

Novel FRET-Based Src Biosensor Reveals Mechanisms of Src Activation and Its Dynamics in Focal Adhesions

Graphical Abstract

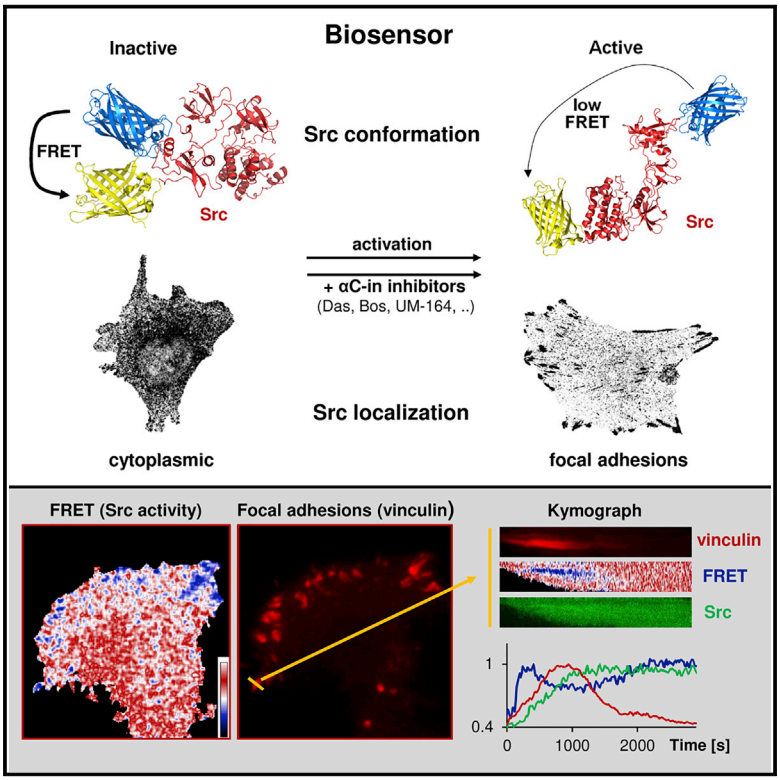

Highlights

- FRET-based Src biosensor was developed and functionally verified
- Src activatory mutations induce opening of Src structure
- Src inhibitors differentially affect Src structure and its cellular localization
- Src activity is high in FAs and increases/decreases during FA assembly/disassembly

Authors

Lenka Koudelková, Andreea Csilla Pataki, Ondřej Tolde, ..., Kurt Anderson, Jan Brábek, Daniel Rosel

Correspondence

rosel@natur.cuni.cz

In Brief

Koudelková et al. developed and functionally verified a Src kinase biosensor. The biosensor represents a unique tool to monitor Src structure, activity, and localization both *in vitro* and in cells. Using the biosensor, the action of Src inhibitors and Src dynamics in focal adhesions was described.

Koudelková et al., 2019, Cell Chemical Biology *26*, 255–268
February 21, 2019
https://doi.org/10.1016/j.chembiol.2018.10.024

CellPress

Cell Chemical Biology
Article

Novel FRET-Based Src Biosensor Reveals Mechanisms of Src Activation and Its Dynamics in Focal Adhesions

Lenka Koudelková,[1,5] Andreea Csilla Pataki,[1,5] Ondřej Tolde,[1] Vojtech Pavlik,[1,3] Max Nobis,[2] Jakub Gemperle,[1] Kurt Anderson,[2,4] Jan Brábek,[1] and Daniel Rosel[1,6,*]
[1]Charles University, Faculty of Science - BIOCEV, Department of Cell Biology, Vestec 252 50, Czech Republic
[2]Cancer Research UK, Beatson Institute, Glasgow G611BD, UK
[3]Present address: Contipro, Dolní Dobrouč 561 02, Czech Republic
[4]Present address: The Francis Crick Institute, London NW11AT, UK
[5]These authors contributed equally
[6]Lead Contact
*Correspondence: rosel@natur.cuni.cz
https://doi.org/10.1016/j.chembiol.2018.10.024

SUMMARY

Src kinase plays an important role in a multitude of fundamental cellular processes and is often found deregulated in tumors. Active Src adopts an open conformation, whereas inactive Src is characterized by a very compact structure stabilized by inhibitory intramolecular interactions. Taking advantage of this spatial regulation, we constructed a fluorescence resonance energy transfer (FRET)-based Src biosensor and analyzed conformational changes of Src following Src activation and the spatiotemporal dynamics of Src activity in cells. We found that activatory mutations either in regulatory or kinase domains induce opening of the Src structure. Surprisingly, we discovered that Src inhibitors differ in their effect on the Src structure, some counterintuitively inducing an open conformation. Finally, we analyzed the dynamics of Src activity in focal adhesions by FRET imaging and found that Src is rapidly activated during focal adhesion assembly, and its activity remains steady and high throughout the life cycle of focal adhesion and decreases during focal adhesion disassembly.

INTRODUCTION

The product of the *c-src* proto-oncogene, Src kinase, is the founding member of the Src family nonreceptor tyrosine kinases. Src plays crucial roles in migration, mechanosensing, and mitogenic and anti-apoptotic signaling, thus precise control of Src activation is necessary to avoid tumor transformation (Yeatman, 2004; Frame et al., 2002; Playford and Schaller, 2004). Despite the mechanisms of negative control, enhanced expression and/or activation of Src is commonly observed in various tumors (e.g., colon carcinomas, breast carcinomas, pancreatic carcinomas) (Irby and Yeatman, 2000; Giaccone and Zucali, 2008). Under the circumstances of elevated or aberrant Src kinase activity, numerous Src substrates become phosphorylated. These Src phosphorylated substrates have been implicated in induction of tumorigenesis and development of malignant cell phenotype (Yeatman, 2004; Frame et al., 2002; Playford and Schaller, 2004). Even though a vast number of Src kinase substrates have been already identified, the exact mechanism of Src-mediated transformation has not been completely elucidated.

Seven functionally and structurally important regions can be described in Src. From the N terminus it is the SH4 domain, unique domain, SH3 domain, SH2 domain, CD linker, catalytic domain, and C-terminal tail containing a key regulatory residue Y527 (chicken Src numbering). SH3 and SH2 domains serve not only for binding of signaling partners (e.g., p130Cas, FAK, paxillin, STAT3) but they also play an important role in downregulating Src kinase activity (Superti-Furga et al., 1993). Structural studies have shown that active Src adopts an open conformation, whereas inactive Src is characterized by very compact structure, with the SH3 and SH2 domains turned inward, and packed against the catalytic domain on the side opposite to the catalytic cleft (Xu et al., 1997). The compact and inactive conformation of Src is maintained by three main intramolecular interactions: (1) SH2 domain binding of phosphorylated Y527, (2) binding of SH3 domain to a part of the CD linker, (3) binding of SH3 domain to the N-terminal lobe of the catalytic domain (Brabek et al., 2002; Cooper et al., 1986; Xu et al., 1997). The release of the intramolecular regulatory interaction of SH2 domain with phosphorylated Y527 leads to the opening of Src structure and the kinase domain adopts an active conformation (Cowan-Jacob et al., 2005). The mechanism of SH3 domain-mediated negative regulatory interactions, and especially their effect on Src structure, remains less understood.

The current model for Src regulation proposes a correlation between structural condensation of the protein backbone and catalytic activity (Cowan-Jacob et al., 2005). Upon external stimuli or mutagenesis, intramolecular regulatory interactions are disturbed, the conformation loosens, and Src kinase domain becomes activated. Taking advantage of these conformational changes, we

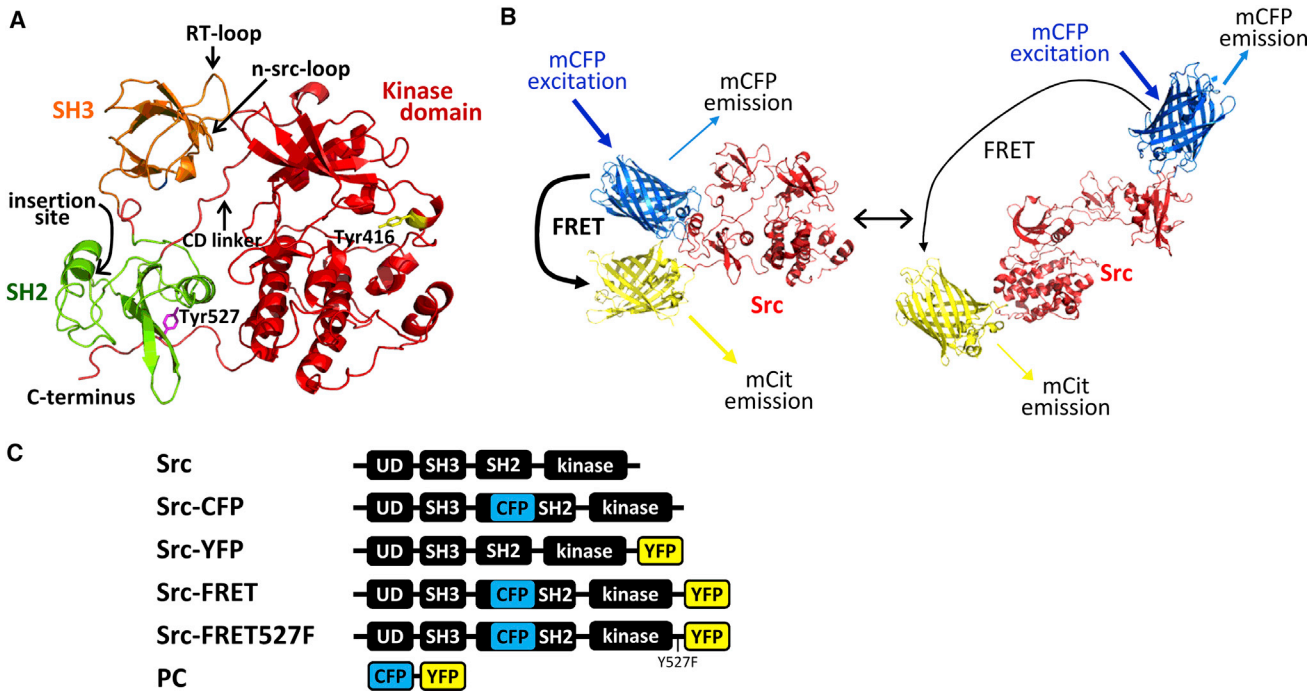

Figure 1. Design of Src-FRET Biosensor

(A) Structure of inactive Src with critical residues and motives depicted.

(B) Model of Src biosensor action. Compact, inactive conformation of Src biosensor gives high FRET between inserted mCFP and mCit fluorophores (left). Upon activation, the Src structure loosens and the FRET decreases (right). Linkers between the fluorophores and the kinase are not depicted. The structure models were created according to PDB structures PDB: 1FMK, 1Y57, 2H5P, 1F0B.

(C) Schematic representation of the different Src and control constructs used in this study. UD, unique domain; CFP, mECFP/(mTurquoise2); YFP, mCit.

constructed a genetically encoded intramolecular FRET-based Src biosensor and analyzed conformational changes of Src following Src activation induced by Src mutagenesis or upon external chemical or mechanical stimulation of cells. Using FRET imaging we further analyzed the spatiotemporal dynamics of Src activation in focal adhesions.

RESULTS

Design and Construction of Src-FRET Biosensor

According to known structures of active and inactive Src, the greatest spatial distance between any two parts of the Src molecule after its activation is the distance between C terminus and SH2 domain (Cowan-Jacob et al., 2005, Figures 1A and 1B). We thus decided to insert the FRET pair of fluorescence proteins in this area of Src. The donor fluorophore was inserted in the loop between βD and βE strands of the SH2 domain (Xu et al., 1997). This loop is oriented outward of the compact structure of Src and is on the opposite side to the SH2 ligand binding site. To minimize potential disrupting effect of the fluorescence protein insertion on the SH2 domain fold, two highly flexible linker peptides (eight, eleven amino acids) were added to the donor fluorescence protein inserted to SH2 domain. The acceptor fluorescence protein was inserted at the very C terminus of the Src molecule (seven-amino-acids-long linker peptide). To minimize dimerization artifacts, monomeric versions of fluorescent proteins mCFP and mCitrine (mCit) were chosen as donor and acceptor fluorophores, respectively.

Given the proposed design, the following constructs were prepared: the full-length chicken *c-src* gene with mCFP inserted into the SH2 domain (Src-CFP), chicken *c-src* with mCit linked to the C terminus of Src (Src-YFP), complete biosensor construct with both mCFP and mCit inserted (Src-FRET), complete biosensor construct where Src kinase was activated by mutation of Tyr527 to Phe (Y527F, Src-FRET527F), and positive control construct (PC; no Src, only mCFP and mCit connected by short linker for maximum FRET) (Figure 1C). The constructs were expressed in HEK cells and the relative levels of an activatory phosphorylation of Tyr416 within the activation loop were determined. Immunoblot analysis indicated that none of the constructs with wild-type (WT) Src showed any significant difference ($p > 0.45$) in relative phosphorylation of Tyr416, which suggests that the insertion of the fluorophores has no effect on basal activity of Src kinase (Figure 2A). In contrast, the biosensor construct with activated Src exhibits a significant increase (approximately 2-fold) of relative Tyr416 phosphorylation, confirming its activated status.

In the prepared biosensor variants, the FRET between the incorporated fluorophores was measured with a FRET steady-state approach (Figure 2B). Fluorescence spectra were recorded in fresh cell lysates at an excitation wavelength of 433 nm, which excites the mCFP donor, and FRET ratio was calculated as ratio of fluorescence intensity at 480 nm (mCFP emission peak) and

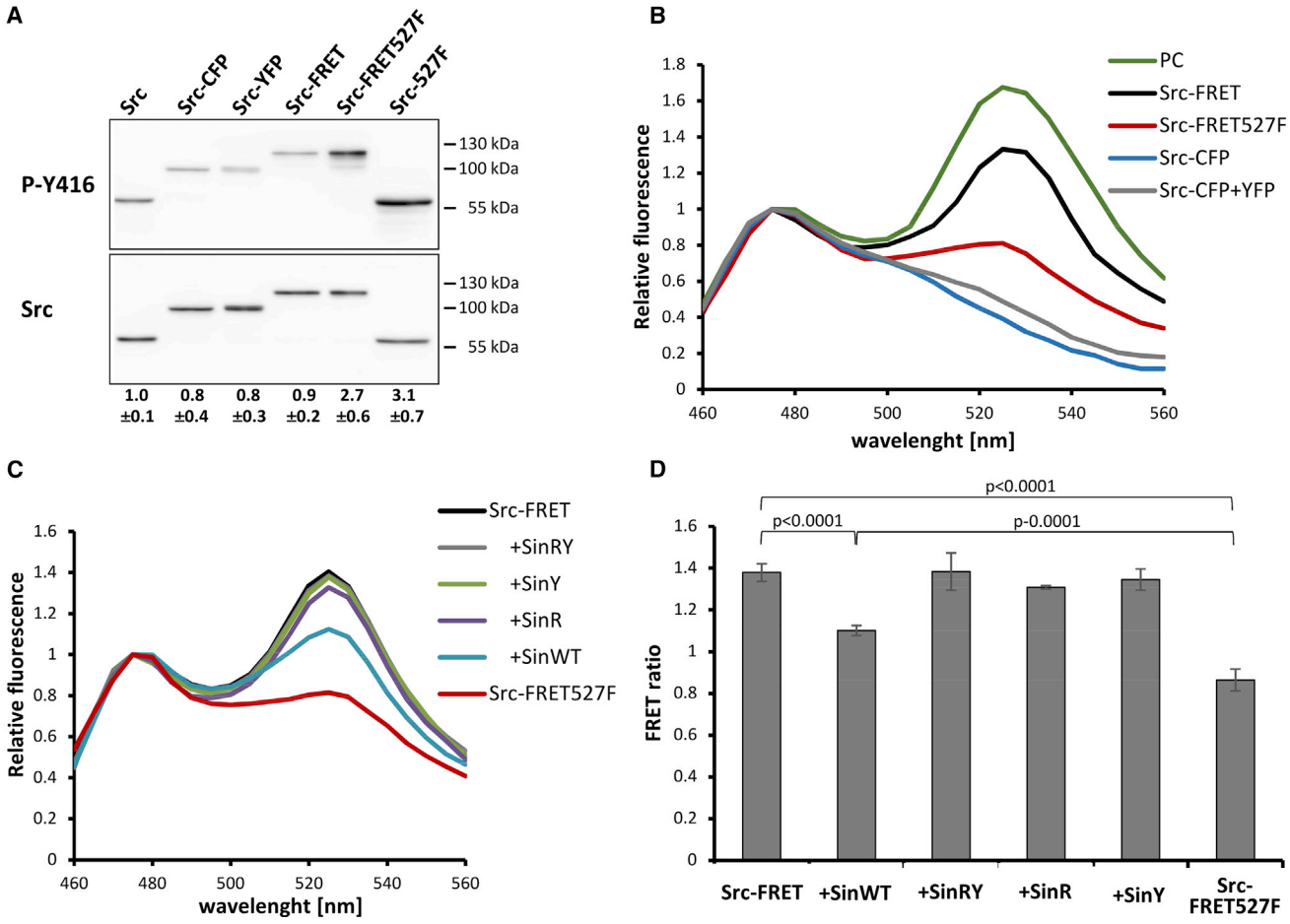

Figure 2. Insertion of the Fluorophores into Src Has No Significant Effect on Src Activation

HEK293FT cells expressing Src constructs were lysed and analyzed for Tyr416 phosphorylation and emission spectra.

(A) Representative matched pair of immunoblots showing detection of activated Src (P-Y416 antibody) and total Src. Numbers indicate ratio of Tyr416 phosphorylation and Src signal (mean ± SD, out of minimum five independent experiments) normalized to unmanipulated Src.

(B) Representative emission spectra normalized to emission maximum of mCFP.

(C and D) The biosensor variants were transfected into HEK293FT cells and native cell lysates were supplemented with purified glutathione S-transferase (GST) SinWT (FRET + SinWT), GST-SinY (FRET + SinY), GST-SinR (FRET + SinR), GST-SinRY (FRET + SinRY), or GST alone (FRET, FRET527F). After 30 min of incubation, fluorescence emission spectra were recorded. (C) Representative emission spectra normalized to emission maximum of mCFP. (D) Bar graph represents ratio of normalized mCit (525 nm) and mCFP (475 nm) emission. The data are shown as mean ± SD out of a minimum three independent experiments performed in triplicate. p values indicate statistical significance calculated by one-way ANOVA and followed by Tukey's post hoc test.

525 nm (mCit emission peak). FRET ratio of Src-FRET construct on average reached approximately 73% of the maximum FRET within the theoretical range, given by the difference in FRET ratio between the PC and Src-CFP, and was significantly ($p < 0.0001$) different from the FRET ratio of Src-FRET527F reaching approximately 33% of the maximum FRET. This shows that the dynamic range of the Src-FRET biosensor is at least 40% of the theoretical dynamic range for the FRET of the mCFP and mCit pair, indicating that the Src-FRET biosensor can effectively monitor structural changes following Src activation. Importantly, the fluorescence spectra from cells transfected simultaneously by Src-CFP and Src-YFP constructs closely resemble spectra from cells transfected by Src-CFP only, confirming that the FRET observed in Src-FRET and Src-FRET527 is a result of an intramolecular FRET (Figure 2B).

Src-FRET Biosensor Is Responsive to Interaction-Based Activation

The inactive structure of Src is maintained by intramolecular interactions mediated by SH2 and SH3 domains (Xu et al., 1997). It was previously shown that cooperative binding of peptides derived from Src interactor Sin to Src SH2 and SH3 domains can activate Src (Alexandropoulos and Baltimore, 1996). The Src-FRET biosensor represents an excellent tool to test the effect of peptides competing with intramolecular binding sequences on the compactness of Src structure. We thus analyzed the effect of purified variants of Sin-derived peptides on FRET of the Src-FRET biosensor *in vitro*. In agreement with the study of Alexandropoulos and Baltimore (1996), our results showed that Sin peptide carrying both SH2 and SH3 binding sites (SinWT) effectively promotes the

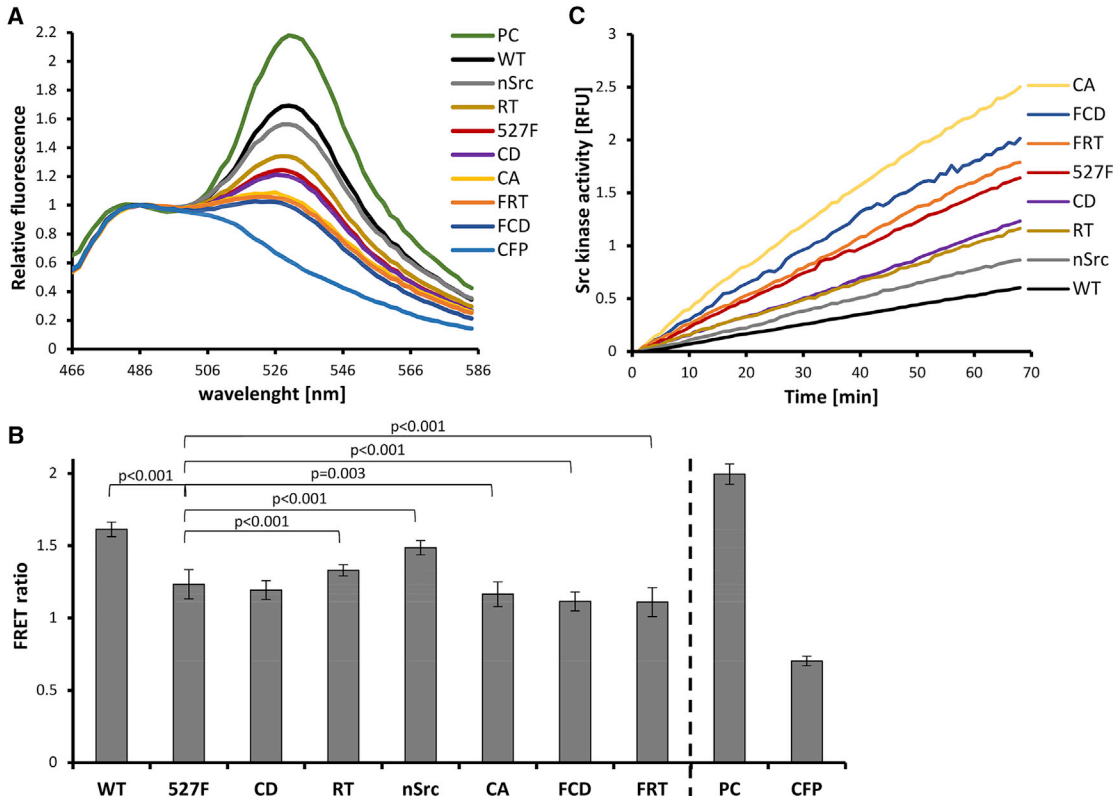

Figure 3. Src-FRET Biosensor Is Responsive to Activatory Mutations

The biosensor variants were transfected into U2OS cells and the fluorescence emission spectra were recorded.

(A) Representative emission spectra normalized to emission maximum of mCFP.

(B) Bar graph represents ratio of normalized mCit (530 nm) and mCFP (480 nm) emission. The data are shown as mean ± SD out of minimum three independent experiments performed in triplicate. p values indicate statistical significance compared with FRET ratio of Src-FRET527F (527F) variant of the biosensor as calculated by one-way ANOVA and followed by Tukey's post hoc test. PC (positive control) and CFP (Src-CFP) indicates maximum and minimum FRET achievable by the biosensor, respectively.

(C) Kinetic analysis of kinase activity of the biosensor variants using Omnia kinase assay. Representative graph is shown.

decrease in FRET ratio of the Src biosensor, whereas the Sin peptides mutated either in SH2 (SinY), SH3 (SinR), or both SH2 and SH3 binding sites (SinRY) have no effect (Figures 2C and 2D).

The Effect of Src Mutations on Compactness of Src Structure

A large number of mutations activating the oncogenic potential of Src were described throughout the history of Src proto-oncogene analysis; however, the effect of many of these mutations on the overall structure/compactness of Src is not known. This is especially true for mutations affecting SH3-mediated intramolecular interactions. To this end, we introduced several mutations known to affect Src activity into the biosensor and analyzed their effect on FRET and kinase activity. We prepared three biosensor variants carrying activatory mutations affecting the SH3-mediated regulation of Src: (1) Src-FRET-RT biosensor with mutation in the RT loop of SH3 domain inhibiting its interaction with kinase domain (Thr96/Ile + Arg95/Trp; Miyazaki et al., 1999); (2) Src-FRET-nSrc with mutation in the n-Src loop of SH3 domain inhibiting its interaction with kinase domain (Asp117/Asn; Miyazaki et al., 1999); (3) Src-FRET-CD with mutation in the CD linker inhibiting its binding to SH3 domain (Pro250/Gly, Lys249/Asp; Gonfloni et al., 1997). In addition, we prepared a biosensor variant Src-FRET-CA carrying mutation within the kinase domain (Glu381(376)/Gly) shown to constitutively activate Src, although the mechanism of the activation is unknown (Bjorge et al., 1995), and two double-mutant variants combining the activatory Tyr527 to Phe mutation uncoupling the SH2-mediated regulation with either RT loop or CD linker mutations (Src-FRET-FRT and Src-FRET-FCD, respectively).

The mutated variants of the biosensor were transiently expressed in U2OS cells and the effect of the mutations on FRET and Src kinase activity was analyzed. All mutated variants have shown significantly lower FRET ($p < 0.001$) than the non-mutated biosensor (Figures 3A and 3B). When compared with the FRET ratio of the SH2-activated Src-FRET527F, the biosensors show four different levels of FRET. First, there is a group not significantly different ($p > 0.323$) from Src-FRET527F, which includes Src-FRET527F itself and Src-FRET-CD variants. The Src-FRET-CA and the double-mutated Src-FRET-FRT and Src-FRET-FCD variants form a group of biosensors with FRET significantly lower

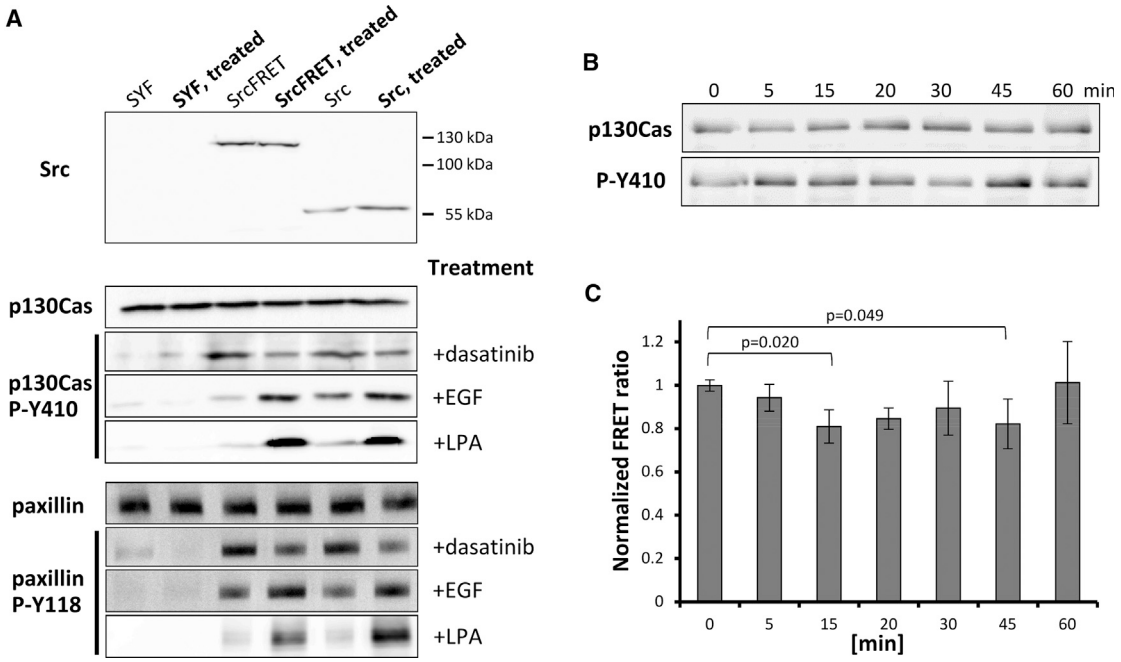

Figure 4. Src-FRET Biosensor Effectively Responds to Treatments Activating and Inhibiting Src

(A) SYF cells and SYFs stably expressing Src-FRET biosensor (SrcFRET) or c-Src (Src) were incubated for 30 min ± 150nM dasatinib, for 12 hr ± 100 ng/mL EGF or for 2 hr ± 10 μM LPA. Cells were then lysed and analyzed for expression and phosphorylation of Src substrates paxillin and p130Cas. Representative blots from three independent experiments are shown.

(B and C) SYF cells stably expressing SrcFRET-WT biosensor were seeded on fibronectin-coated flexible membrane, incubated for 24 hr, and then subjected to 20% static stretch for indicated times. (B) Cells were lysed and analyzed by western blotting against phosphorylated Y410 in the p130Cas (P-Y410) substrate domain. Representative blot from three independent experiments is shown. (C) Cells were lysed and in native cell lysates the FRET was analyzed as a ratio of FRET fluorescence intensity (λ_{ex} 433 nm, λ_{em} 530 nm) and fluorescence intensity of mCFP (λ_{ex} 433 nm, λ_{em} 480 nm). FRET ratio of unstretched cells (0 min) was arbitrary set to 1. The data are shown as mean ± SD out of minimum three independent experiments performed in triplicate. p values indicate statistical significance compared with unstretched cells (0 min) as calculated by one-way ANOVA and followed by Tukey's post hoc test.

($p < 0.004$) than Src-FRET527F. The biosensor variants with activating mutations directly within SH3 domain exhibit an intermediate level of FRET decrease. The Src-FRET-RT exhibits FRET levels close to, but significantly higher ($p < 0.001$) than, that of the Src-FRET527F group. The mutations within the nSrc-loop, the Src-FRET-nSrc variant, have the least effect on compactness of Src structure as its FRET is significantly higher than even that of the Src-FRET-RT ($p < 0.001$). In addition to FRET, the effect of the mutations on Src kinase activity was evaluated using a kinetic kinase assay. The sensitivity of the assay was not sufficient to confirm the four different levels of the Src activity, as indicated by the FRET analysis. When compared with kinase activity of Src-FRET527F, only Src-FRET-CA has shown significantly higher kinase activity ($p = 0.009$) and Src-FRET-WT together with Src-FRET-nSrc exhibited significantly lower kinase activity ($p < 0.001$ and $p = 0.013$, respectively). The kinase activities of individual Src-FRET variants, however, exhibited, in an inverse manner, similar trends to the FRET (Figures 3C and S1). This could be in part because the variants with higher activity were on average expressed less than Src-FRET-WT and thus could be masked by the residual activity of endogenous Src family kinases in the cell lysates.

Taken together, these data show that the biosensor can effectively monitor even small changes in activity of Src and that mutations affecting SH3-mediated intramolecular interactions of Src also result in the opening of Src structure.

Src-FRET Biosensor Is Functionally Equivalent to Src

The initial testing of the biosensor has shown that the biosensor expressed in HEK and U2OS cells can monitor structural changes of Src following activation via mutation of regulatory Y527 or using an SH2-SH3 competing peptide. HEK and U2OS cells express a low but not negligible amount of endogenous Src and thus are not optimal for testing functional relevance of the biosensor for Src signaling. Therefore, we stably expressed the Src-FRET biosensor in SYF fibroblasts (nulls for Src family kinases, Src, Yes, and Fyn; Klinghoffer et al., 1999) and analyzed the effect of Src-FRET biosensor activation on phosphorylation of Src substrates p130Cas and paxillin. The phosphorylation of both p130Cas and paxillin was virtually absent in untransfected SYFs. In contrast, expression of Src-FRET biosensor in SYFs resulted in substantial phosphorylation of both p130Cas and paxillin. This phosphorylation was significantly increased upon stimulation of the cells with epidermal growth factor (EGF) or lysophosphatidic acid (LPA) and, conversely, inhibited when treated with Src kinase inhibitor dasatinib (Figure 4A). These results indicate that Src-FRET biosensor effectively phosphorylates known Src substrates and responds both to

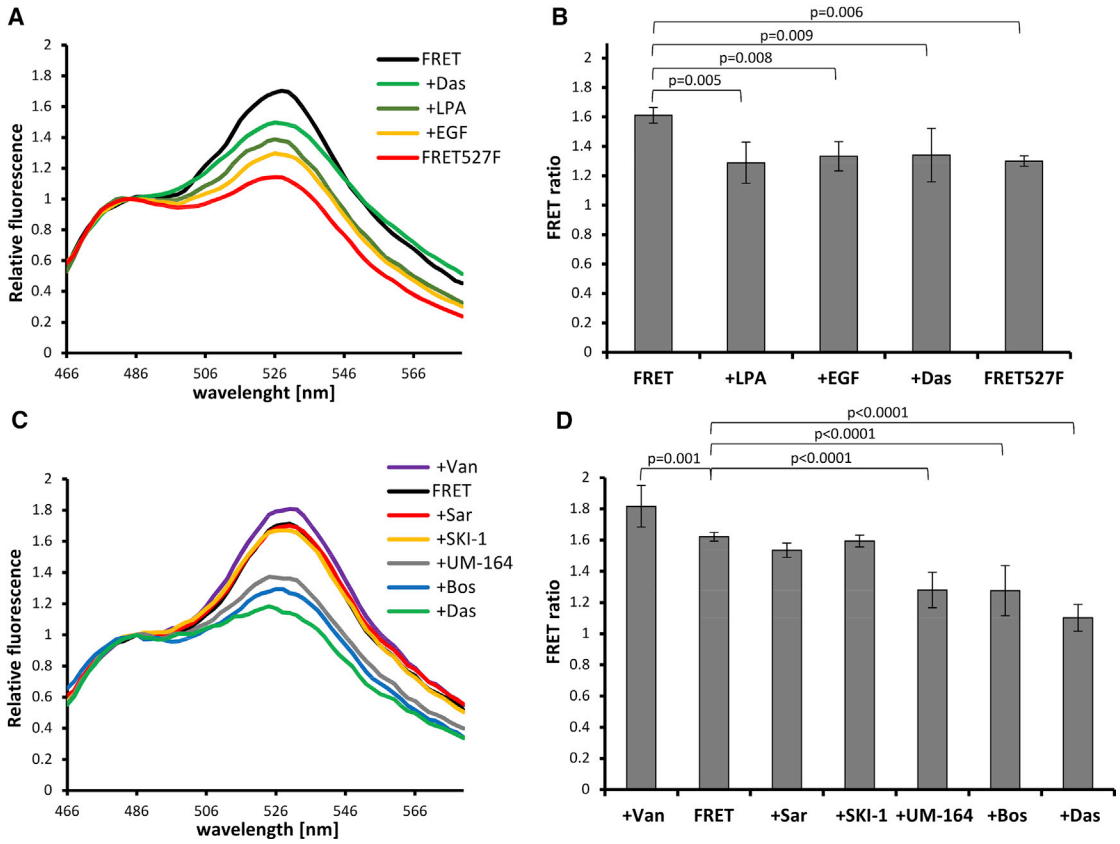

Figure 5. Src-FRET Biosensor Is Responsive to Activatory and Inhibitory Treatments in Cells

Src-FRET biosensor (FRET) and biosensor with activating Tyr527 to Phe mutation (FRET527F) were stably expressed in SYF cells. SYFs expressing the FRET-WT biosensor were incubated for 10 min with 10 μM LPA (serum starved, +LPA), 24 hr with 100 ng/mL EGF (serum starved, +EGF), 60 min with 500 μM sodium orthovanadate (+Van), or for 60 min with Src kinase inhibitors: 100 nM dasatinib (+Das), 4 μM saracatinib (+Sar), 1 μM bosutinib (+Bos), 100 nM UM164 (+UM-164), or 10 μM SKI-1 (+SKI-1). (A and C) Representative emission spectra. Relative fluorescence represents fluorescence intensity normalized to emission maximum of mCFP. (B and D) Bar graph represents ratio of normalized mCit (530 nm) and mCFP (480 nm) emission. The data are shown as mean ± SD out of minimum three independent experiments performed in triplicate. p values indicate statistical significance compared with FRET ratio from untreated cells (FRET) as calculated by one-way ANOVA and followed by Tukey's post hoc test.

physiological signals activating Src and to inhibition by Src inhibitor.

Src Activation Dynamics upon Mechanical Stimulation

P130Cas, an adaptor protein and Src substrate, was shown to function as a mechanosensor. Its substrate domain can be mechanically stretched, and this exposes tyrosine residues within the domain for Src-mediated phosphorylation (Janostiak et al., 2014b; Sawada et al., 2006). Interestingly, static mechanical stretch of cells induces biphasic tyrosine phosphorylation of p130Cas with maximum at 15 and 45 min after the stretch (Janostiak et al., 2014a). However, the role of Src in tension-mediated phosphorylation was not clearly addressed. We stretched SYFs expressing Src-FRET biosensor and analyzed Src activity in the cells by monitoring the total level of FRET and phosphorylation of p130Cas. We found that FRET of the biosensor is significantly decreased 15 min and 45 min after the stretch (Figures 4B and 4C). The dynamics of Src activation upon static stretch thus reflects the biphasic dynamics of p130Cas phosphorylation and shows that mechanical stimulation of cells activates Src.

The Effect of Inhibitors on Src Structure

Having established that the Src-FRET biosensor functions effectively as Src in cells and responds to mechanical stimuli, we then examined the effect of LPA, EGF, and compounds known to inhibit Src on the FRET ratio of the Src-FRET biosensor in cells. The treatment of SYFs expressing the Src-FRET biosensor with both EGF and LPA resulted in significant decrease of FRET ratio, indicating and confirming activation of the biosensor in the cells upon EGF and LPA treatments (Figures 5A and 5B; compare with Figure 4A). Surprisingly, treatment with dasatinib induced significant decrease of FRET, indicating open conformation of Src, despite inactivating Src kinase activity (Figures 5 and S2). It was previously shown for Hck and Src kinases that binding of specific ligands targeting the ATP-binding pocket results in increased accessibility of SH2 and SH3 domains to intermolecular binding, which could be responsible for the observed dasatinib-induced opening of Src structure (Leonard et al., 2014). Therefore, we decided to analyze a panel of Src inhibitors for the effect on compactness of the Src-FRET biosensor. All kinase inhibitors tested effectively inhibited the Src kinase as monitored

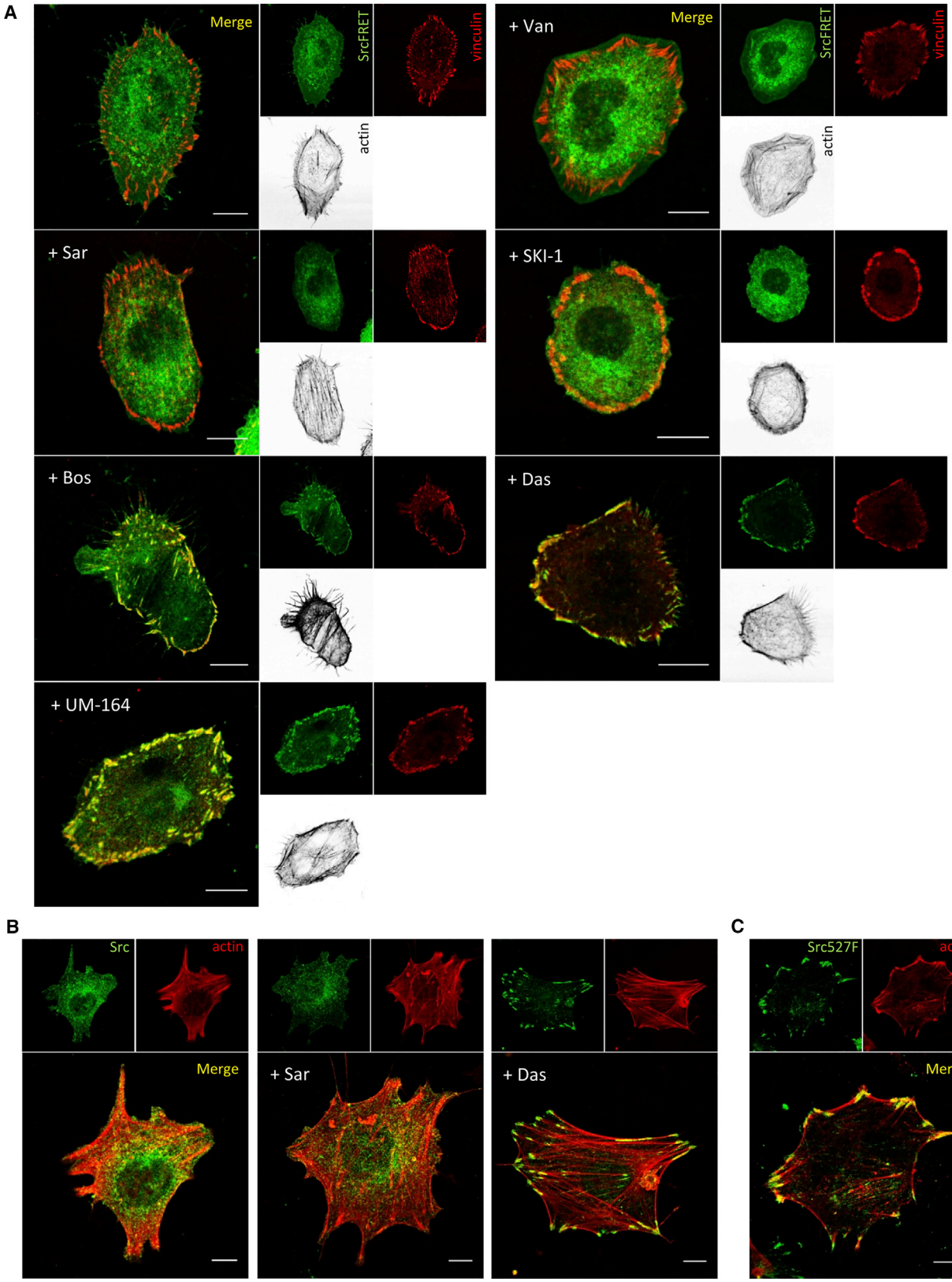

(legend on next page)

by decreased phosphorylation of Src substrate p130Cas and decreased phosphorylation of Src in the activation loop on Tyr416. Along with dasatinib, bosutinib and UM-164 also significantly lowered ($p < 0.05$) the FRET ratio of the biosensor. In contrast, treatment of the cells with saracatinib and SKI-1 had no effect on FRET (Figures 5C and 5D). We also tested the effect of sodium orthovanadate, which inhibits Src kinase activity by preventing P-Tyr527 dephosphorylation (Ryder and Gordon, 1987), and found that it significantly increases the FRET ratio of the biosensor (Figures 5C and 5D). This is consistent with the increased Tyr527 phosphorylation and subsequent induction of closed conformation of Src.

When analyzing the effect of inhibitors on the FRET ratio of the Src-FRET biosensor we noticed a substantial difference in pattern of Src-FRET biosensor localization in the cells. Strikingly, the inhibitors that induced opened conformation of the Src-FRET biosensor (dasatinib, UM-164, bosutinib) showed high enrichment in focal adhesions resembling the localization of the 527F activated Src (Figure 6; Fincham and Frame, 1998). In contrast, treatment of cells with inhibitors not affecting the FRET ratio of the Src-FRET biosensor (SKI-1, saracatinib) and with sodium orthovanadate did not visibly change the localization pattern of the Src-FRET biosensor, which remained mostly cytoplasmic.

Taken together, the inhibitors analyzed exhibited two distinct phenotypes of action on Src. The first group, represented by dasatinib, bosutinib, and UM-164, induces opened conformation of Src and enrichment of the Src-FRET biosensor in focal adhesions, whereas saracatinib and SKI-1 do not affect Src conformation and localization. Our results further indicate that opened conformation of Src and not its kinase activity is required for its targeting to focal adhesions.

Analysis of Src Activation Using FRET Imaging

The Src-FRET biosensor proved its potential in analyzing Src activity upon Src mutagenesis and activation/inhibition of the cells by chemical and mechanical cues. Because of its design it can provide not only information about Src activity but also about Src intracellular localization dynamics. Therefore, we next focused on monitoring Src activation dynamics in cells. To overcome the higher demand for the donor fluorophore stability and brightness in long-term life imaging experiments, we replaced mCFP in the Src-FRET construct for mTurquoise2 (Goedhart et al., 2012). When expressed in cells, the resulting Src-FRET(T) construct monitored Src activation status after the treatment with LPA or EGF in a similar manner to its mCFP counterpart, although, when compared with maximum FRET of PC (mTurquoise2-mCit), its dynamic range was somehow smaller than that of the mCFP variant of the biosensor (Figure S3). The Src-FRET(T) biosensor exhibited, however, much brighter and more stable donor fluorescence, effectively enabling us to monitor dynamics of Src activation status in live cells.

To analyze the dynamics of Src activation in focal adhesions, U2OS cells were transiently co-transfected with the Src-FRET(T) biosensor and mCherry-FAT (focal adhesion targeting domain of FAK) or mCherry-vinculin constructs, and FRET and mCherry signals were analyzed live by total internal reflection fluorescence (TIRF) microscopy during later stages of cell spreading. The focal adhesions were detected using the mCherry signal of the mCherry-FAT or mCherry-vinculin fusion constructs. The cell body was detected as the mCit signal of the Src-FRET(T) biosensor. The FRET was analyzed by the sensitized emission approach and quantified as nF/I_{CFP} according to Xia and Liu (2001). On average, we found that FRET in focal adhesions is about 20% lower than in surrounding cytoplasm, showing highly significant ($p < 2x10^{-26}$) and localized activation of Src in focal adhesions (Figure 7D). In fact, in the cell area illuminated by the TIRF evanescent field, the active Src conformation was detected almost exclusively in focal adhesions (Video S1). Analysis of Src activation dynamics revealed that, during the initial phase of focal adhesion formation, characterized by increasing intensity signal of mCherry-FAT or mCherry-vinculin, the FRET is high at the beginning but decreases progressively, reaching its minimal values mostly before the mCherry signal reaches its maximum intensity (Figures 7 and S4). The FRET remains low throughout the mature stage of focal adhesion, characterized by stable intensity of the mCherry signal, and gradually increases during focal adhesion disassembly (Figures 7B and 7C).

Even though Src is locally activated in focal adhesions, we did not observe any enrichment of Src, detected as mCit signal, in any stage of focal adhesion life cycle (Figures 7B and 7C). This indicates high dynamics of Src in focal adhesions. Fluorescence recovery after photobleaching (FRAP) analysis revealed that Src-FRET(T) biosensor dynamics in focal adhesions is indeed very high, with average half-time recovery 0.90 ± 0.57 s (Figure S5). This is well in agreement with single-molecule analyses showing 1-s residency time of Src in focal adhesions (Machiyama et al., 2015).

DISCUSSION

Understanding the precise regulation of Src in living cells is the key to understanding Src-dependent signal transduction and to development of effective therapeutic approaches targeting Src. Aberrant Src activation leads to weakening of cell-cell and cell-matrix contacts, increased expression of matrix metalloproteinases, cytoskeleton remodeling, and elevated adhesion turnover resulting in enhanced cell motility (Mitra and Schlaepfer, 2006; Guarino, 2010). Even though the role of Src kinase in cellular locomotion has been broadly documented, the exact mechanism and spatiotemporal dynamics of Src activation within invasive and adhesive structures has not been sufficiently elucidated.

To monitor Src activity in cells, several attempts have already been made, including FRET-based substrate biosensors (Ting et al., 2001; Wang et al., 2005), a biosensor based on a monobody targeting the SH3 domain of Src (Gulyani et al., 2011),

Figure 6. The Effect of Src Inhibitors on Src-FRET Biosensor Localization

SYF cells stably expressing SrcFRET-WT biosensor (A), c-Src (B), or activated Src (Src527F) (C) were directly stained or incubated for 60 min with 500 μM sodium orthovanadate (+Van), or for 60 min with Src kinase inhibitors: 100 nM dasatinib (+Das), 4 μM saracatinib (+Sar), 1 μM bosutinib (+Bos), 100 nM UM-164 (+UM-164), or 10 μM SKI-1 (+SKI-1). Cells were then fixed and stained for vinculin (focal adhesions marker, red in A), F-actin (gray in A or red in B and C), or Src (mCit fluorescence in A or anti-Src antibody in B and C, green) and imaged by confocal microscopy. Scale bar 10 μm.

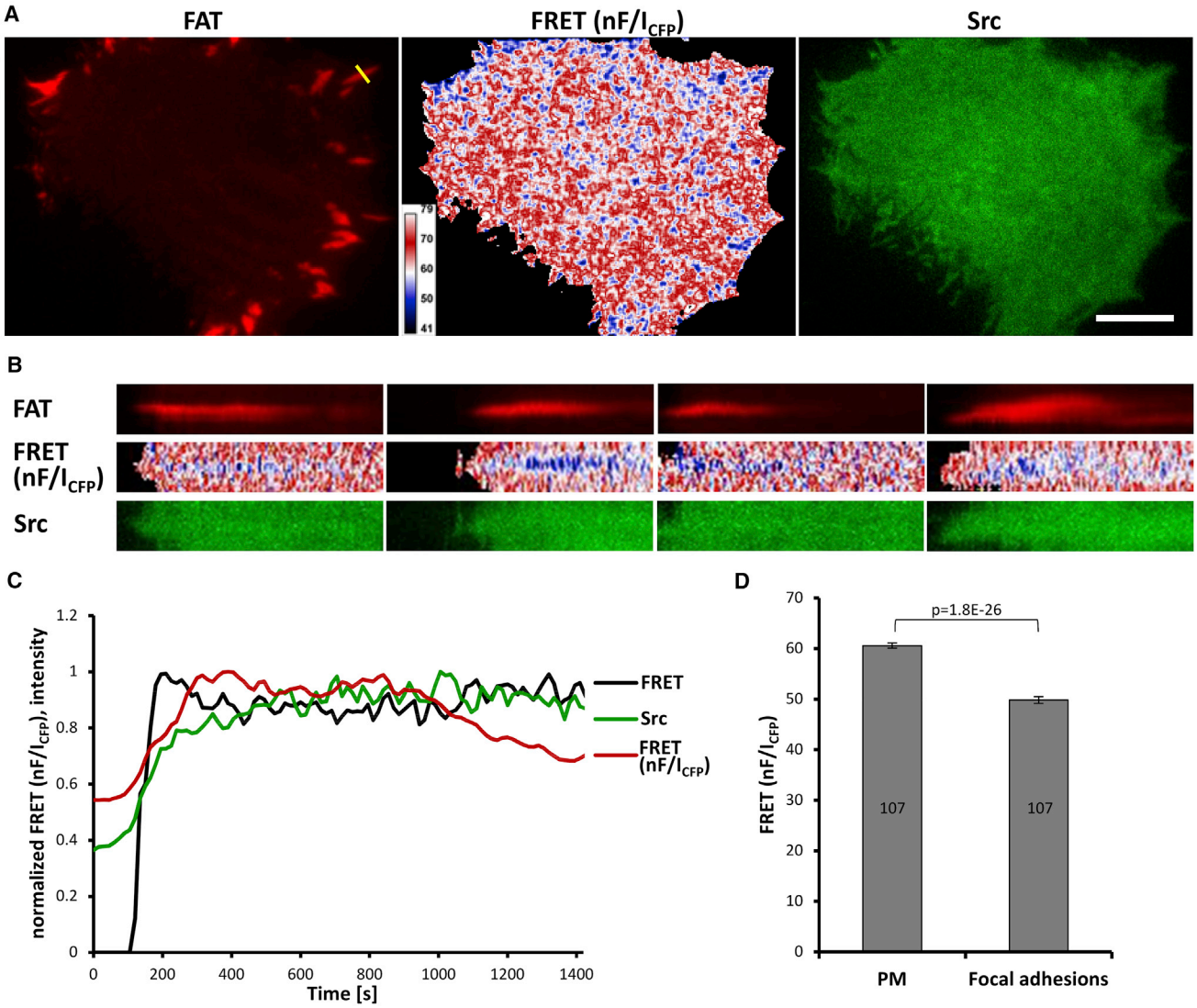

Figure 7. Src Activity in Focal Adhesions

U2OS cells transiently co-expressing mTurquoise2-based Src-FRET(T) and mCherry-FAT were imaged live.

(A) Representative cell image showing focal adhesions (FAT, mCherry signal, red), Src activity map (FRET, nF/I_{CFP}), and Src-FRET(T) localization (Src, mCit signal, green). The yellow line across focal adhesion indicates the place of the first (left) kymograph analysis. Scale bar, 10 μm.

(B) Representative kymographs (out of 20) of FAT, Src-FRET(T) localization, and Src-FRET(T) activity dynamics in focal adhesions within 1,800-s time frame.

(C) Representative graph showing dynamics of mCherry-FAT (FAT), Src-FRET(T) (Src) localization, and Src-FRET(T) activity (FRET, nF/I_{CFP}) dynamics in focal adhesion. The data correspond to the first (left) kymograph in (B) and are normalized to maximum values.

(D) The bar graph shows average FRET (nF/I_{CFP}) ± SEM in focal adhesions and random regions of plasma membrane (PM) of similar size as the focal adhesions. The number in the bar graphs indicates the number of individual measurements. p value indicates statistical significance as calculated by one-way ANOVA.

and biarsenical dye staining of a tetracysteine motif introduced into the SH2 domain (Irtegun et al., 2014). All approaches provided valuable information about Src activity in the cells. However, and unlike our biosensor, they do not provide combined information about the activity and intracellular localization of diverse subpopulations of Src molecules at one time. An approach similar to ours was adopted to monitor the activation of Src family kinase Lck (Paster et al., 2009; Stirnweiss et al., 2013). The authors designed a FRET biosensor consisting of a full backbone of Lck with enhanced yellow fluorescent protein inserted at the very C terminus and enhanced cyan fluorescent protein inserted either between SH3 and SH2 domains (Paster et al., 2009) or between the unique and SH3 domain (Stirnweiss et al., 2013). Our Src-FRET biosensor uses the same insertion site for the acceptor fluorophore (the very C terminus of Src) but differs in the insertion site of the donor fluorophore. Insertion into the linker between SH3 and SH2 domains could not be used for Src, since the linker is critical to couple communication between SH3 and SH2 domains and mutation of this linker leads to activation of Src (Young et al., 2001). Insertion between the SH3 and unique domain is in our opinion less optimal than our solution, as it is sterically more distant from the C terminus

than our insertion into the SH2 domain and would lead to less efficient FRET. In agreement with these assumptions, in the *in vitro* steady-state FRET measurements (ratio of relative FRET and CFP fluorescence) our biosensor exhibits a higher dynamic range than that of Lck (Stirnweiss et al., 2013).

Src-Activating Mutations and Their Effect on Compactness of Src Structure

Throughout the 40-year history of studying Src kinase, many mutations activating Src were described. The crystallographic data have come with clear evidence that mutations affecting SH2-mediated intramolecular interactions lead to the opening of Src structure (Cowan-Jacob et al., 2005). However, there was no clear evidence on the effect of SH3-mediated intramolecular interactions or activatory mutations in the kinase domain on Src structure. Our data show that mutations inhibiting SH3-CD linker interaction lead to the opening of the Src structure to a similar extent to the Tyr527 to Phe mutation uncoupling the SH2-mediated regulation. Mutations affecting the interaction of SH3 domain with the N-terminal lobe of the kinase domain also effectively induced opening of Src structure but to a lesser extent. Importantly, the effect of the mutations inhibiting the SH2- and SH3-mediated intramolecular interactions is additive, indicating a high degree of independence of these negative intramolecular interactions in regulation of Src kinase. Surprisingly, the activatory mutation within the kinase domain Glu381(376)/Gly opens the Src structure to a level similar to the analyzed double mutants. The Glu381(376) is located at the C terminus of αE helix in the C lobe of the kinase domain and is not in contact with either the SH2 or SH3 domain in the closed inactive conformation of Src (Xu et al., 1997). Therefore, the effect of Glu381(376)/Gly substitution on opening of the Src structure is indirect. To conclude, the data suggest that activated conformation of the kinase domain negatively affects intramolecular SH2 and SH3 binding to the kinase domain and forces the opened conformation of Src.

Differential Effect of Src Inhibitors on Src Structure

Src kinase inhibition has long been an important target for cancer therapy (Rosel et al., 2013). The known small-molecule Src kinase inhibitors are ATP-competitive inhibitors and, according to their binding mode, are generally classified as type I or type II inhibitors; type I bind active and type II bind inactive kinase (Dar and Shokat, 2011). The classification of the inhibitors relies mostly on the position of conserved DFG motif at the beginning of activation segment. The "DFG-in" position, specific for type I inhibitors, represents an active state of the kinase with aspartate of the DFG motif oriented inward toward the active site. When this aspartate is directed outward (DFG-out, type II inhibitors), the phenylalanine of DFG is directed into the active site and the kinase is in inactive conformation (Roskoski, 2016). Besides the position of the DFG, the αC helix orientation is also associated with active (αC-in) and inactive (αC-out) state of the kinase (Leonard et al., 2014).

The inhibitors analyzed exhibited two distinct phenotypes of action on Src. The first group, represented by dasatinib, bosutinib, and UM-164, induced opened conformation of Src and enrichment of the Src-FRET biosensor in focal adhesions. This phenotype closely resembled the phenotype 527F activated Src, indicating that the phenotype is associated with active rather than inactive conformation of Src. The second group, represented by saracatinib and SKI-1, had no effect on either compactness of Src structure or Src-FRET biosensor localization to focal adhesions. Dasatinib and bosutinib represent type I Src inhibitors binding Src in DFG-in, αC-in conformation (Leonard et al., 2014; Roskoski, 2016; Tong et al., 2017). UM-164 (DAS-DFGO2) and saracatinib are type II inhibitors (DFG-out) that differ in their effect on the αC helix position, UM-164 binding Src with αC-in and saracatinib with αC-out conformation (Roskoski, 2016; Tong et al., 2017). For SKI-1 we could not ascertain its binding mode to Src in the literature. The common denominator of the effect of all three inhibitors promoting the opened structure of Src is induction of αC-in conformation. Similarly, it was shown that inhibitors stabilizing αC-in active conformation of the kinase domain greatly increase accessibility of the Src SH3 domain for intramolecular interactions, indicating a potential opening of Src structure (Leonard et al., 2014).

Within the kinase inhibitors tested, dasatinib, UM-164, and bosutinib significantly reduced phosphorylation of the regulatory Tyr527. The dephosphorylation of Tyr527 releases the SH2-mediated intramolecular regulatory interaction and should lead to Src opening. This raises the question of whether the effect of the inhibitors on the Src structure is direct or mediated by inhibition of Csk kinase, the master regulator of Src and, as previously shown, also effectively inhibited by dasatinib (Karaman et al., 2008). The fact that only αC-in inhibitors (dasatinib, bosutinib, and UM-164) induce Src structure opening would appear to be in line with their pronounced effect on Tyr527 dephosphorylation (Figure S2A). However, we noticed that dasatinib significantly decreases FRET of not only the WT Src-FRET biosensor but also of the activated Src-FRET527F biosensor, which is by definition insensitive to Csk regulation. Conversely, SKI-1 surprisingly increased FRET of the activated Src-FRET527F biosensor, indicating closing of the Src structure (Figures S2B–S2D). We conclude that the effect of the inhibitors on the opening of the Src structure is primarily independent of Csk inhibition. We hypothesize that the high increased dephosphorylation of Tyr527 in cells treated with αC-in inhibitors, when compared with saracatinib and SKI-1, could be in part a consequence of inhibitor-induced opening of the Src structure and subsequent faster dephosphorylation of phospho-Tyr527 by tyrosine phosphatases. In addition, we hypothesize that SKI-1 inhibitor forces closed conformation of the kinase domain and this subsequently induces partial closing of the activated Src-FRET527F. Overall, the data are consistent with the direct effect of inhibitors on kinase domain conformation, which affects the global compactness of the Src structure: namely, kinase domain in active conformation characterized by αC helix-in orientation induces global opening of Src. In agreement with this, activatory mutation in the kinase domain (Glu381(376)/Gly) promotes Src structure opening (Figure 3). Finally, our results show that the Src-FRET biosensor could be used as a tool to distinguish between the modes of binding/action of new inhibitors without the need for resolving the structure of the Src-inhibitor complex. In this sense, we can conclude that SKI-1 inhibitor binds Src in its inactive conformation with αC-out orientation of the αC helix.

The Src-FRET biosensor unraveled two classes of Src inhibitors differing in their effect on the Src structure and subcellular

localization. Conceivably, biological activity of inactivated Src kinase would differ for inactivated Src with opened conformation, with both SH2 and SH3 domains unrestricted for binding their targets, and inactivated Src in closed conformation. Therefore, the two classes of Src inhibitors would have different effects on intracellular signaling and thus potentially diverse therapeutic outcomes.

Src as a Potential Mechanosensor

The Src-FRET biosensor monitors Src activity through conformational changes, opening of the compact structure of inactive Src, following Src activation. It is thus intriguing that mechanical stimulation of cells leads to the opening of the Src structure. The dynamics of Src opening upon mechanical stretching of the cells follows the pattern of p130Cas phosphorylation. P130Cas was shown to function as a primary mechanosensor; upon mechanical stretch its substrate domain unfolds and exposes cryptic tyrosines that are subsequently phosphorylated by Src (Sawada et al., 2006). The spatiotemporal resolution achieved in our cell-stretching experiments did not allow us to distinguish whether the Src opening precedes p130Cas phosphorylation or vice versa. However, the cellular stretch-mediated opening of Src indicates that Src could act as a primary mechanosensor, which is directly mechanical activated by local forces. Interestingly, the substrate-based Src biosensors revealed that local Src activation in response to mechanical perturbation can be very fast, which is in agreement with the concept of Src being a sensor of local mechanical tension (Wang et al., 2005; Na et al., 2008). In this context, our experimental setup relies on average status of the biosensor molecules in cell populations. Therefore, it could not detect fast local mechanical tension-mediated activation of the molecules but is rather dependent on accumulation of the activated molecules in time. To further ascertain the function of Src as a mechanosensor, live cell FRET imaging with the Src-FRET biosensor under controlled exertion of local mechanical forces on the cells together with *in vitro* experiments showing on a molecular level the tension-mediated opening of Src structure and the induction of its kinase activity are needed.

Src Role in Focal Adhesions

It has been well established that Src has mostly uniform distribution in cells, with a significant fraction localized on membrane, and that activated Src is enriched in focal adhesions (Machiyama et al., 2015). Src localization to focal adhesions requires intact SH2 domain and is mediated by FAK (Klinghoffer et al., 1999; Machiyama et al., 2015; Wu et al., 2016). This mechanism of Src focal adhesion targeting implies a requirement for opened conformation of Src, which we have confirmed with our biosensor. Surprisingly, no enrichment of Src was observed in any stage of the focal adhesion life cycle. This raises a question about the mechanism of Src activation in focal adhesions. We envision three potential mechanisms of Src structure opening in focal adhesions. First, local dephosphorylation of tyrosine 527 would release the intramolecular SH2 binding and allow for its intermolecular bindings (e.g., to phosphorylated FAK). This would induce opened conformation of Src and activate the kinase. Second, and analogous to our observation with Sin-derived peptides, simultaneous binding of SH2 and SH3 domain to their target sites within focal adhesion proteins opens Src and activates the kinase. Third, opened conformation of Src is achieved by direct mechanical tension. We propose that the opening of Src structure could be achieved by dynamic mechanical tension in focal adhesions, generated by the molecular clutch phenomenon (Mitchison and Kirschner, 1988), which is transmitted to Src molecules, anchored on N terminus to plasma membrane, through intermolecular SH2 domain binding. According to the molecular clutch theory, individual molecules of mechanosensors in focal adhesions, either directly or indirectly contacting the F-actin retrograde flow, are subject to very fast fluctuations of increased tension when contacting the F-actin flow and released tension when disengage from the flow. This tension would release the SH3-mediated intramolecular interaction and force the full activation of the kinase. Interestingly, we found that Src is extremely dynamic in focal adhesions. This is inconsistent with the model of Src targeting through simultaneous binding of SH2 and SH3 domains to focal adhesion proteins, which would be expected to stabilize Src in focal adhesions to a level similar to focal adhesion's resident proteins exhibiting focal adhesion half-time recovery time in mouse fibroblasts ranging from 12 s (p130Cas; Janostiak et al., 2014a) to 50 s (Talin; Stutchbury et al., 2017). On the contrary, Src exhibits high dynamics and localized activation in focal adhesions without detectable enrichment. This is in line with the hypothesis of tension-mediated opening of Src.

The dynamics of Src activation in focal adhesions was previously analyzed using substrate-based FRET biosensors (Wu et al., 2016). The data suggested that assembly of focal adhesions and Src activation are practically concurrent and that focal adhesion disassembly is preceded by another wave of Src activation. We do not see waves of Src activation in focal adhesions but rather a steady activation level of Src throughout the mature, stable phase of the focal adhesions life cycle and rapid activation or gradual inhibition during focal adhesion assembly and disassembly, respectively. Both biosensors differ in their modes of action. Our biosensor relies on correlation between compactness of Src structure and its activity, which we have confirmed under all experimental setups tested. Nevertheless, we cannot rule out a specific condition in live cells where opened conformation is not strictly reflected by higher kinase activity. In contrast, the substrate biosensors monitor the kinase activity through the level of specific substrate phosphorylation. This, however, depends on local combination of kinase and counteracting phosphatases activities. Putting both observations together, we propose the following model of Src's role in the focal adhesions life cycle. Src is locally and rapidly activated during focal adhesion assembly and phosphorylates its substrates. Its activity remains high during the mature stage of focal adhesion cycle but is counteracted by phosphatases that stabilize the level of phosphorylation of the Src substrates in focal adhesions. The disassembly is potentially initiated by decreased activity of phosphatases, inducing hyperphosphorylation of Src targets and subsequent disassembly of focal adhesions (Figure S6).

There is indirect evidence that increased Src-dependent phosphorylation destabilizes localization of proteins in focal adhesion or even destabilizes the focal adhesions themselves (Figure S6). Among other things, it was shown that (1) cells lacking the tyrosine phosphatase Shp2 exhibited increased turnover of focal adhesions (von Wichert et al., 2003); (2) increased tyrosine

phosphorylation of paxillin is associated with more dynamic focal adhesions and is absent from stable fibrillar adhesions (Zaidel-Bar et al., 2007); and that (3) Src phosphorylation of ARHGAP42 on tyrosine 376 increases the dynamics of focal adhesions (Luo et al., 2017). In addition, Src was shown to phosphorylate with slow dynamics p130Cas of Tyr12 within the SH3 domain, inhibiting its binding capacity and SH3-mediated anchoring of p130Cas to focal adhesions (Branis et al., 2017; Gemperle et al., 2017). The mutational analysis of Tyr12 further suggested that its phosphorylation destabilizes focal adhesions and induces the migratory phenotype of the cell (Janostiak et al., 2011). Besides phosphorylation-dependent loss of binding to focal adhesions, Src phosphorylation-stimulated p130Cas ubiquitination and its subsequent degradation was shown as another mechanism regulating focal adhesion's dynamics (Teckchandani et al., 2014).

SIGNIFICANCE

In our study we have analyzed conformational changes of Src following Src activation and the spatiotemporal dynamics of Src activity in cells. To better understand the biology of Src proto-oncogene, we took advantage of the known structural changes associated with Src activation to design, construct, and functionally verify a genetically encoded FRET-based Src biosensor. Using the biosensor, we found that activatory mutations in SH3 domain, CD linker, or kinase domain induce the opening of Src structure similarly to the oncogenic Tyr257 to Phe mutation. Further, we discovered that Src inhibitors exhibit two distinct phenotypes of action on Src. The first group of inhibitors, characterized by inducing an αC helix-out conformation of the kinase domain, has no effect on Src structure or localization. The second group, inducing αC helix-in conformation, surprisingly and counterintuitively leads to opened conformation of Src and its localization to focal adhesions. Finally, we analyzed the dynamics of Src activity in focal adhesions by FRET imaging. Based on these results, we propose a model for the role of Src-dependent phosphorylation in focal adhesions, according to which Src-dependent tyrosine phosphorylation of focal adhesion proteins drives the assembly phase of focal adhesions. It remains stable during the maturation of focal adhesions due to counteracting activity of tyrosine phosphatases. Hyperphosphorylation of the Src targets in focal adhesions, potentially due to decreased phosphatase activity, induces disassembly of focal adhesions and is followed by Src inactivation. The Src-FRET biosensor represents a unique tool to monitor Src structure, activity, and localization both *in vitro* and in cells and hence could help to identify mechanisms of action of new Src targeting drugs as well as to investigate various aspects of Src signaling in live cells.

STAR★METHODS

Detailed methods are provided in the online version of this paper and include the following:

- KEY RESOURCES TABLE
- CONTACT FOR REAGENT AND RESOURCE SHARING
- EXPERIMENTAL MODEL AND SUBJECT DETAILS
  - Cell Lines and Transfection
- METHOD DETAILS
  - DNA Constructs
  - Sin Peptides Purification
  - Immunoblotting
  - Kinase Assay
  - Cell Stretching
  - FRET Steady-State Analysis
  - Fluorescence Microscopy
- QUANTIFICATION AND STATISTICAL ANALYSIS

SUPPLEMENTAL INFORMATION

Supplemental Information includes six figures and one video and can be found with this article online at https://doi.org/10.1016/j.chembiol.2018.10.024.

ACKNOWLEDGMENTS

We gratefully acknowledge Dr. Xuehua Xu and Dr. Joseph Brzostowski for help with the FRET protocol, Dr. Tomas Vomastek for the gift of cell lines, and Dr. Katerina Kuzelova for the gift of SKI-1 inhibitor. This work was funded by Czech Science Foundation grant 15 07321S, and in part by project Center for Tumor Ecology (reg. no. CZ.02.1.01/0.0/0.0/16_019/0000785) supported by the Operational Programme Research, Development and Education. We acknowledge the IMCF at BIOCEV, institution supported by grants LM2015062 and CZ.02.1.01/0.0/0.0/16_013/0001775, MEYS CR.

AUTHOR CONTRIBUTIONS

L.K. and A.C.P. performed most of the experiments and analyzed the results. O.T. performed the FRET imaging experiments. V.P. and D.R. performed the original cloning and analyses in HEK cells. J.G. and M.N. analyzed the results. D.R., J.B., and K.A. conceived the experiments and wrote the manuscript. All authors reviewed the manuscript.

DECLARATION OF INTERESTS

D.R. and J.B. have filed a Czech Republic patent application on the Src-FRET biosensor. The authors have no other financial or non-financial competing interests.

Received: June 21, 2018
Revised: September 12, 2018
Accepted: October 26, 2018
Published: December 13, 2018

REFERENCES

Alexandropoulos, K., and Baltimore, D. (1996). Coordinate activation of c-Src by SH3- and SH2-binding sites on a novel p130Cas-related protein. Sin. Genes Dev. *10*, 1341–1355.

Bjorge, J.D., Bellagamba, C., Cheng, H.C., Tanaka, A., Wang, J.H., and Fujita, D.J. (1995). Characterization of two activated mutants of human pp60c-src that escape c-Src kinase regulation by distinct mechanisms. J. Biol. Chem. *270*, 24222–24228.

Brabek, J., Mojzita, D., Novotny, M., Puta, F., and Folk, P. (2002). The SH3 domain of Src can downregulate its kinase activity in the absence of the SH2 domain-pY527 interaction. Biochem. Biophys. Res. Commun. *296*, 664–670.

Branis, J., Pataki, C., Sporrer, M., Gerum, R.C., Mainka, A., Cermak, V., Goldmann, W.H., Fabry, B., Brabek, J., and Rosel, D. (2017). The role of focal adhesion anchoring domains of CAS in mechanotransduction. Sci. Rep. *7*, 46233.

Cooper, J.A., Gould, K.L., Cartwright, C.A., and Hunter, T. (1986). Tyr527 is phosphorylated in pp60c-src: implications for regulation. Science *231*, 1431–1434.

Cowan-Jacob, S.W., Fendrich, G., Manley, P.W., Jahnke, W., Fabbro, D., Liebetanz, J., and Meyer, T. (2005). The crystal structure of a c-Src complex in an active conformation suggests possible steps in c-Src activation. Structure *13*, 861–871.

Dar, A.C., and Shokat, K.M. (2011). The evolution of protein kinase inhibitors from antagonists to agonists of cellular signaling. Annu. Rev. Biochem. *80*, 769–795.

Feige, J.N., Sage, D., Wahli, W., Desvergne, B., and Gelman, L. (2005). PixFRET, an ImageJ plug-in for FRET calculation that can accommodate variations in spectral bleed-throughs. Microsc. Res. Tech. *68*, 51–58.

Fincham, V.J., and Frame, M.C. (1998). The catalytic activity of Src is dispensable for translocation to focal adhesions but controls the turnover of these structures during cell motility. EMBO J. *17*, 81–92.

Fonseca, P.M., Shin, N.Y., Brabek, J., Ryzhova, L., Wu, J., and Hanks, S.K. (2004). Regulation and localization of CAS substrate domain tyrosine phosphorylation. Cell Signal *16*, 621–629.

Frame, M.C., Fincham, V.J., Carragher, N.O., and Wyke, J.A. (2002). v-Src's hold over actin and cell adhesions. Nat. Rev. Mol. Cell Biol. *3*, 233–245.

Gemperle, J., Hexnerova, R., Lepsik, M., Tesina, P., Dibus, M., Novotny, M., Brabek, J., Veverka, V., and Rosel, D. (2017). Structural characterization of CAS SH3 domain selectivity and regulation reveals new CAS interaction partners. Sci. Rep. *7*, 8057.

Giaccone, G., and Zucali, P.A. (2008). Src as a potential therapeutic target in non-small-cell lung cancer. Ann. Oncol. *19*, 1219–1223.

Goedhart, J., von, S.D., Noirclerc-Savoye, M., Lelimousin, M., Joosen, L., Hink, M.A., van, W.L., Gadella, T.W., Jr., and Royant, A. (2012). Structure-guided evolution of cyan fluorescent proteins towards a quantum yield of 93%. Nat. Commun. *3*, 751.

Gonfloni, S., Williams, J.C., Hattula, K., Weijland, A., Wierenga, R.K., and Superti-Furga, G. (1997). The role of the linker between the SH2 domain and catalytic domain in the regulation and function of Src. EMBO J. *16*, 7261–7271.

Guarino, M. (2010). Src signaling in cancer invasion. J. Cell Physiol *223*, 14–26.

Gulyani, A., Vitriol, E., Allen, R., Wu, J., Gremyachinskiy, D., Lewis, S., Dewar, B., Graves, L.M., Kay, B.K., Kuhlman, B., et al. (2011). A biosensor generated via high-throughput screening quantifies cell edge Src dynamics. Nat. Chem. Biol. *7*, 437–444.

Irby, R.B., and Yeatman, T.J. (2000). Role of Src expression and activation in human cancer. Oncogene *19*, 5636–5642.

Irtegun, S., Wood, R., Lackovic, K., Schweiggert, J., Ramdzan, Y.M., Huang, D.C., Mulhern, T.D., and Hatters, D.M. (2014). A biosensor of SRC family kinase conformation by exposable tetracysteine useful for cell-based screening. ACS Chem. Biol. *9*, 1426–1431.

Janostiak, R., Brabek, J., Auernheimer, V., Tatarova, Z., Lautscham, L.A., Dey, T., Gemperle, J., Merkel, R., Goldmann, W.H., Fabry, B., and Rosel, D. (2014a). CAS directly interacts with vinculin to control mechanosensing and focal adhesion dynamics. Cell Mol. Life Sci. *71*, 727–744.

Janostiak, R., Pataki, A.C., Brabek, J., and Rosel, D. (2014b). Mechanosensors in integrin signaling: the emerging role of p130Cas. Eur. J. Cell Biol. *93*, 445–454.

Janostiak, R., Tolde, O., Bruhova, Z., Novotny, M., Hanks, S.K., Rosel, D., and Brabek, J. (2011). Tyrosine phosphorylation within the SH3 domain regulates CAS subcellular localization, cell migration, and invasiveness. Mol. Biol. Cell *22*, 4256–4267.

Karaman, M.W., Herrgard, S., Treiber, D.K., Gallant, P., Atteridge, C.E., Campbell, B.T., Chan, K.W., Ciceri, P., Davis, M.I., Edeen, P.T., et al. (2008). A quantitative analysis of kinase inhibitor selectivity. Nat. Biotechnol. *26*, 127–132.

Klinghoffer, R.A., Sachsenmaier, C., Cooper, J.A., and Soriano, P. (1999). Src family kinases are required for integrin but not PDGFR signal transduction. EMBO J. *18*, 2459–2471.

Leonard, S.E., Register, A.C., Krishnamurty, R., Brighty, G.J., and Maly, D.J. (2014). Divergent modulation of Src-family kinase regulatory interactions with ATP-competitive inhibitors. ACS Chem. Biol. *9*, 1894–1905.

Luo, W., Janostiak, R., Tolde, O., Ryzhova, L.M., Koudelkova, L., Dibus, M., Brabek, J., Hanks, S.K., and Rosel, D. (2017). ARHGAP42 is activated by Src-mediated tyrosine phosphorylation to promote cell motility. J. Cell Sci. *130*, 2382–2393.

Machiyama, H., Yamaguchi, T., Sawada, Y., Watanabe, T.M., and Fujita, H. (2015). SH3 domain of c-Src governs its dynamics at focal adhesions and the cell membrane. FEBS J. *282*, 4034–4055.

Mitchison, T., and Kirschner, M. (1988). Cytoskeletal dynamics and nerve growth. Neuron *1*, 761–772.

Mitra, S.K., and Schlaepfer, D.D. (2006). Integrin-regulated FAK-Src signaling in normal and cancer cells. Curr. Opin. Cell Biol. *18*, 516–523.

Miyazaki, K., Senga, T., Matsuda, S., Tanaka, M., Machida, K., Takenouchi, Y., Nimura, Y., and Hamaguchi, M. (1999). Critical amino acid substitutions in the Src SH3 domain that convert c-Src to be oncogenic. Biochem. Biophys. Res. Commun. *263*, 759–764.

Na, S., Collin, O., Chowdhury, F., Tay, B., Ouyang, M., Wang, Y., and Wang, N. (2008). Rapid signal transduction in living cells is a unique feature of mechanotransduction. Proc. Natl. Acad. Sci. U. S. A. *105*, 6626–6631.

Paster, W., Paar, C., Eckerstorfer, P., Jakober, A., Drbal, K., Schutz, G.J., Sonnleitner, A., and Stockinger, H. (2009). Genetically encoded Forster resonance energy transfer sensors for the conformation of the Src family kinase Lck. J. Immunol. *182*, 2160–2167.

Playford, M.P., and Schaller, M.D. (2004). The interplay between Src and integrins in normal and tumor biology. Oncogene *23*, 7928–7946.

Rosel, D., Brabek, J., Vesely, P., and Fernandes, M. (2013). Drugs for solid cancer: the productivity crisis prompts a rethink. Onco. Targets Ther. *6*, 767–777.

Roskoski, R., Jr. (2016). Classification of small molecule protein kinase inhibitors based upon the structures of their drug-enzyme complexes. Pharmacol. Res. *103*, 26–48.

Ryder, J.W., and Gordon, J.A. (1987). In vivo effect of sodium orthovanadate on pp60c-src kinase. Mol. Cell Biol. *7*, 1139–1147.

Sawada, Y., Tamada, M., Dubin-Thaler, B.J., Cherniavskaya, O., Sakai, R., Tanaka, S., and Sheetz, M.P. (2006). Force sensing by mechanical extension of the Src family kinase substrate p130Cas. Cell *127*, 1015–1026.

Stirnweiss, A., Hartig, R., Gieseler, S., Lindquist, J.A., Reichardt, P., Philipsen, L., Simeoni, L., Poltorak, M., Merten, C., Zuschratter, W., et al. (2013). T cell activation results in conformational changes in the Src family kinase Lck to induce its activation. Sci. Signal *6*, ra13.

Stutchbury, B., Atherton, P., Tsang, R., Wang, D.Y., and Ballestrem, C. (2017). Distinct focal adhesion protein modules control different aspects of mechanotransduction. J. Cell Sci. *130*, 1612–1624.

Superti-Furga, G., Fumagalli, S., Koegl, M., Courtneidge, S.A., and Draetta, G. (1993). Csk inhibition of c-Src activity requires both the SH2 and SH3 domains of Src. EMBO J. *12*, 2625–2634.

Teckchandani, A., Laszlo, G.S., Simo, S., Shah, K., Pilling, C., Strait, A.A., and Cooper, J.A. (2014). Cullin 5 destabilizes Cas to inhibit Src-dependent cell transformation. J. Cell Sci. *127*, 509–520.

Ting, A.Y., Kain, K.H., Klemke, R.L., and Tsien, R.Y. (2001). Genetically encoded fluorescent reporters of protein tyrosine kinase activities in living cells. Proc. Natl. Acad. Sci. U. S. A. *98*, 15003–15008.

Tolde, O., Rosel, D., Janostiak, R., Vesely, P., and Brabek, J. (2012). Dynamics and morphology of focal adhesions in complex 3D environment. Folia Biol. (Praha) *58*, 177–184.

Tong, M., Pelton, J.G., Gill, M.L., Zhang, W., Picart, F., and Seeliger, M.A. (2017). Survey of solution dynamics in Src kinase reveals allosteric cross talk between the ligand binding and regulatory sites. Nat. Commun. *8*, 2160.

von Wichert, G., Haimovich, B., Feng, G.S., and Sheetz, M.P. (2003). Force-dependent integrin-cytoskeleton linkage formation requires downregulation of focal complex dynamics by Shp2. EMBO J. *22*, 5023–5035.

Wang, Y., Botvinick, E.L., Zhao, Y., Berns, M.W., Usami, S., Tsien, R.Y., and Chien, S. (2005). Visualizing the mechanical activation of Src. Nature *434*, 1040–1045.

Wu, Y., Zhang, K., Seong, J., Fan, J., Chien, S., Wang, Y., and Lu, S. (2016). n-situ coupling between kinase activities and protein dynamics within single focal adhesions. Sci. Rep. *6*, 29377.

Xia, Z., and Liu, Y. (2001). Reliable and global measurement of fluorescence resonance energy transfer using fluorescence microscopes. Biophys. J. *81*, 2395–2402.

Xu, W., Harrison, S.C., and Eck, M.J. (1997). Three-dimensional structure of the tyrosine kinase c-Src. Nature *385*, 595–602.

Yeatman, T.J. (2004). A renaissance for SRC. Nat. Rev. Cancer *4*, 470–480.

Young, M.A., Gonfloni, S., Superti-Furga, G., Roux, B., and Kuriyan, J. (2001). Dynamic coupling between the SH2 and SH3 domains of c-Src and Hck underlies their inactivation by C-terminal tyrosine phosphorylation. Cell *105*, 115–126.

Zaidel-Bar, R., Milo, R., Kam, Z., and Geiger, B. (2007). A paxillin tyrosine phosphorylation switch regulates the assembly and form of cell-matrix adhesions. J. Cell Sci. *120*, 137–148.

STAR★METHODS

KEY RESOURCES TABLE

REAGENT or RESOURCE	SOURCE	IDENTIFIER
Antibodies		
Mouse monoclonal anti-Src (clone 184Q20)	Invitrogen	Cat#AHO1152
Rabbit polyclonal anti-phospho-Src (pY418)	Sigma	Cat#S1940
Rabbit polyclonal anti-phospho-Src (pY529)	Sigma	Cat#S2065
Mouse monoclonal anti-p130Cas (clone 21/p130Cas)	BD Transduction Laboratories	Cat#610272
Rabbit polyclonal anti-phospho-p130Cas (pY410)	Cell Signaling	Cat#4011
Mouse monoclonal anti-paxillin (clone 349/paxillin)	BD Transduction Laboratories	Cat#610051
Rabbit polyclonal anti-phospho-paxillin (pY118)	Cell Signaling	Cat#2541
Mouse monoclonal anti-vinculin (clone hVIN-1)	Sigma	Cat#V9131
Bacterial and Virus Strains		
E. coli DH5α	ThermoFisher Scientific	Cat#11319019
E. coli TOP10	ThermoFisher Scientific	Cat#C4040
E. coli BL21	New England BioLabs	Cat#C2530H
Chemicals, Peptides, and Recombinant Proteins		
LPA	Sigma	Cat#L7260
hEGF	Sigma	Cat#E9644
Sodium Orthovanadate	Sigma	Cat#450243
dasatinib	LC Laboratories	Cat#D3307
saracatinib (AZD0530)	BioVision	Cat#1582
bosutinib	LC Laboratories	Cat#B1788
UM-164	Sigma	Cat#SML1928
SKI-1	Abcam	Cat#ab120839
Critical Commercial Assays		
Omnia Y Peptide 2 Kit	ThermoFisher Scientific	Cat#KNZ3021
Experimental Models: Cell Lines		
HEK293FT	ThermoFisher Scientific	Cat#R70007
Phoenix-Eco	ATCC	Cat#CRL-3214
SYF	ATCC	Cat#CRL-2459
U-2 OS	ATCC	Cat#HTB-96
Recombinant DNA		
pBlueScript SK+	Agilent Technologies	Cat#212205
pIRESpuro3	Clontech	Cat#631619
pMSCV-puro	Clontech	Cat#634401
pYES2	ThermoFisher Scientific	Cat#V82520
Software and Algorithms		
Prism 6	GraphPad Software	www.graphpad.com
ImageJ	NIH	imagej.nih.gov/ij/
PixFRET plug-in for ImageJ	Feige et al. (2005)	imagej.nih.gov/ij/plugins
LAS X Software	Leica	www.leica-microsystems.com
Nikon NIS Elements Software	Nikon	www.nikoninstruments.com

CONTACT FOR REAGENT AND RESOURCE SHARING

Further information and requests for resources and reagents should be directed to and will be fulfilled by Daniel Rosel (rosel@natur.cuni.cz).

EXPERIMENTAL MODEL AND SUBJECT DETAILS

Cell Lines and Transfection

HEK293FT (human embryonic kidney, female), Phoenix-Eco (human embryonic kidney, female), SYF (mouse embryonic fibroblasts, sex unspecified (Klinghoffer et al., 1999)), U2OS (human bone osteosarcoma, female) cell lines were cultured in full DMEM (Life Technologies) with 4.5 g/l L-glucose, L-glutamine, and pyruvate, supplemented with 10% fetal bovine serum (Sigma Aldrich), 2% antibiotic–antimycotic (Life Technologies), and 1% MEM non essential amino acids (Life Technologies). Cell transfections were carried out using Lipofectamine® 2000, jet PRIME, or polyethylenimine according to manufacturer instructions. SYFs stably expressing Src biosensor variants were prepared via retrovirus infection using the Src biosensor variants cloned in pMSCV puro vector and the Phoenix retroviral packaging lineage followed by sorting of cell by FACS for YFP.

METHOD DETAILS

DNA Constructs

To generate Src-FRET biosensor, full length chicken Src cDNA was PCR amplified from a source vector (Brabek et al., 2002) using the forward primer (5'-GGATCCATGGGTAGTAGCAAGAGC) and the reverse primer (5'-GAATTCTAGGTTCTCTCCAGGCTGG), and cloned in pYES2 vector. The AatII insertion site for donor fluorophore was created using QuikChange II mutagenesis kit (Stratagene), using the forward (5'-CAAGATCCGCAAGCTGGACGTCAGCGGCGGCTTCTACATC) and reverse (5'-GATGTAGAAGCCGCCGCT GACGTCCAGCTTGCGGATCTTG) primers. The insertion of AatII site resulted in insertion of valine between aminoacid 208 and 209 of chicken Src. The mCFP cDNA was PCR amplified from a source vector (gift from Professor Cerny; PrF UK, Czech Republic) using the forward (5'-GACGTCGGAAGCGGAGGTAGTGGTGGAATGGTGAGCAAGGGCG) and reverse (5'-GACGTCACCTCCA CTGCCGCTACCACTTCCGCCGAGAGTGATCCCG) primers, both included sequence coding for the linker peptides (underlined), and cloned into AatII site in the Src cDNA. The mCit cDNA was PCR amplified from a source vector (gift from Professor Cerny) using the forward primer (5'- GAATTCGGTGGCAGTGGAGGGATGGTGAGCAAGGGCG; underlined sequence coding for the linker peptide) and reverse primer (5'-GAATTCCTACTTGTACAGCTCGTCCATGC), and cloned into EcoRI site in the Src cDNA. To generated mutated versions of the Src-FRET biosensor, the resulted Src-FRET biosensor was first cloned into pBlueScript SK+ using BamHI/ NotI restriction sites and was subsequently mutagenize using QuikChange II mutagenesis kit (Stratagene). The primers used for the mutagenesis were as follows: for Tyr527 to Phe (forward: 5'-CGACAGAGCCCCAGTTCCAGCCTGGAGAGAAC, reverse: 5'-GTTCTCTCCAGGCTGGAACTGGGGCTCTGTCG), for RT loop mutagenesis (forward: 5'-TCCTGGATTGAAACGGACTTGTCCTTC, reverse: 5'-CTCGTAGTCGTAGAGAGCCAC), for n-Src loop mutagenesis (forward: 5'-GAAGGTAACTGGTGGCTGGCTCATTC, reverse: 5'-CGTGTTGTTGACAATCTGCAGGC), for CD linker mutagenesis (forward: 5'-GTCCGGCGACCAGACCCAGGGACTCG, reverse: 5'-GTGGGGCAGACGTTGGTCAG), for kinase domain mutagenesis (forward: 5'-GTGGGGAGGATGAACTACGTGCACC, reverse: 5'-ATAGGCCATGCCGGATGCAATC). The resulted Src-FRET biosensors variants were cloned to expression pIRESpuro3 and pMSCV-puro vectors using BamHI/NotI and BamHI/EcoRV restriction sites, respectively. The mTurquoise2 cDNA with linkers and AatII cloning sites, corresponding to mCFP sequence in the Src-FRET biosensor, was prepared by DNA synthesis (GeneArt, Life Technologies) and after digestion with AatII it was cloned to replace mCFP in the AatII site of Src-FRET constructs. For FRET positive control constructs, both mCFP and mTurquoise2 were PCR amplified from corresponding Src-FRET constructs using the same set of primers (forward: 5'-GAATTCCACCATGGTGAGCAAGGGCG, reverse 5'-GGATCCAGATCTGAGTCCGGACTTGTA CAGCTCGTCCATGC) and cloned into EcoRI/BamHI sites of pIRESpuro3. The mCit was PCR amplified using the forward (5'-GGATCCATGGTGAGCAAGGGCG) and reverse (5'- GCGGCCGCCTTGTACAGCTCGTCCATGC) primers and cloned into BamHI/ NotI sites next to the inserted mCFP or mTurquoise2.

To generate mCherry-FAT construct, FAT domain of mouse FAK PCR amplified from a source vector (Fonseca et al., 2004) using the forward primer (5'- GGATCCATGGGTGTCAAGCTTCAGCC) and reverse (5'- AGATCTGTGTGGCCGTGTCTGC), and cloned in frame to BglII site in pmCherry-C1 vector.

All the constructs were verified by sequencing.

Sin Peptides Purification

The plasmids coding for GST-Sin peptide variants, 92 amino acids long peptides with high affinity binding sites for SH3 and SH2 domain of Src, were kind gift from Dr. Alexandropoulos (Alexandropoulos and Baltimore, 1996). The GST-Sin peptide variants were expressed in *Escherichia coli* BL21, purified using Glutathione Agarose (Thermo Scientific) and bound GST-Sin peptides were eluted with 10 mM glutathione in 50 mM Tris, pH 8.0. The quality of purified peptides was assessed by SDS-PAGE and their quantity was determined densitometrically from Coomassie blue-stained gels using a BSA standard. To determine the effect of GST-Sin peptide variants on Src-FRET biosensor, 40 μg of individual GST-Sin peptides were mixed with native cell lysate of HEK293 cells expressing Src-FRET, incubated for up to 40 minutes with vigorous shaking and the fluorescence spectra were recorded (see "FRET steady-state analysis").

Immunoblotting

Subconfluent cells were washed on ice with 1 x PBS and lysed, using RIPA buffer (0.15M NaCl; 50mM Tris-HCl, pH 7.4; 1% Nonidet P-40; 0.1% SDS; 1% sodium deoxycholate; 5mM EDTA; 50mM NaF). Protein concentration of lysates were determined by using the

DC Protein Assay (Bio-Rad). Protein lysates were diluted in Laemmli sample buffer (0.35M Tris-HCl, pH 6.8; 10% SDS, 40% glycerol; 0.012% bromophenol blue) with 1mM DTT. Protein samples were separated on 10% SDS-polyacrylamide gels and transferred onto nitrocellulose membranes. The membranes were usually cut after the transfer to enable probing for up to 3 proteins of different molecular mass (e.g. 1-2 proteins of interest and a loading control). Membranes were then blocked in Tris-buffered saline, containing 5% non-fat dry milk (or 4% bovine serum albumin depending on the antibody) for 1 h at room temperature to prevent non-specific activity. After blocking, membranes were incubated overnight at 4°C with a primary antibody, washed properly with Tris-buffered saline with 0.1% Tween-20, and incubated for 1 h with a secondary antibody conjugated with horseradish peroxidase. After washing with TTBS, membranes were developed by using the LAS 1000 Single System (Fujifilm).

Kinase Assay

Kinase activity of Src variants was measured using Omnia® Y Peptide 2 Kit (ThermoFisher Scientific). The assay is based on detection of fluorescence increase after kinase-specific substrate phosphorylation. Specifically, substrate peptide is attached to the chelation-enhanced fluorophore Sox. Upon phosphorylation of the peptide by the kinase, Mg^{2+} is chelated to form a bridge between the Sox moiety and the incorporated phosphate group on the tyrosine within the substrate peptide, which consequently causes increase in fluorescence. Kinase assays were performed according to the manufacturer's protocol. Briefly, cells were washed with PBS and lysed in HEPES-Triton buffer (50mM HEPES, pH 7.4; 1% Triton X-100, 1mM DTT, 6mM $MgCl_2$, 6mM $MnCl_2$, protease inhibitors, phosphatase inhibitors). Lysates were clarified by centrifugation. Kinase reactions (in quadruplicates for each variant) was assembled by adding cell lysate (5 μg per well in 386 well-plate), kinase reaction buffer, 0.2mM DTT, 1mM ATP and 10μM peptide substrate. Using plate reader (Tecan 200Pro), reactions were incubated at 30°C and fluorescence intensity was measured (λ_{ex} 360 ± 10 nm /λ_{em} 485 ± 20 nm) at 60 second intervals for 1 hour. The slope of fluorescence intensity increase was determined and normalized to amount of Src construct in a sample (mCit signal, 500/530 nm).

Cell Stretching

Cell stretching experiments were carried out on 10 cm^2 stretchable PDMS chambers (STREX Inc.). The substrates of chambers were coated with 5 μg/ml fibronectin (Invitrogen). Cells were seeded on fibronectin-coated substrates and cultured overnight at 37°C with 5% CO_2. Uniaxial static stretching was performed in the incubator under regular cell culture conditions, using a manual stretcher (STREX Inc.). Cells were stretched for various time intervals (0 min, 5 min, 15 min, 20 min, 30 min, 45 min and 60 min) at an amplitude of 20 % and then immediately lysed in Tris-buffered saline with 1% tritonX-100 with protease and phosphatase inhibitors (SERVA). The lysis buffer has been used as a reference for FRET measurements. The lysate was split in two parts, one was immediately used for FRET measurement, second for immunoblot analysis after adding Laemmli sample buffer (0.35M Tris-HCl, pH 6.8; 10% SDS, 40% glycerol; 0.012% bromophenol blue) with 1mM DTT.

FRET Steady-State Analysis

Cells expressing the biosensor variants were treated for 10 min with 10μM LPA (after overnight serum starvation), 24 hours with 100 ng/ml EGF (after overnight serum starvation), 60 min with either 500μM Sodium Orthovanadate, 100nM dasatinib (LC Laboratories), 4μM saracatinib (BioVision), 1μM bosutinib (LC Laboratories), 100nM UM-164 (Sigma), or 10μM SKI-1 (Abcam). After the treatment cells were lysed in HEPES-Triton buffer (50mM HEPES, pH 7.4; 1% Triton X-100, 1mM DTT, 6mM $MgCl_2$, 6mM $MnCl_2$, protease inhibitors, phosphatase inhibitors, 100μM ATP), and the FRET signal of each sample was determined using a Varioskan Flash (Figure 2; Thermo Scientific) or Tecan 200Pro (all spectral scanning and direct FRET data except Figure 2; PTI, Edison, NJ) spectral scanning fluorescence plate readers. To record FRET fluorescence spectra, the cell lysates were excited at an excitation wavelength of mCFP (433 ± 5 nm Varioskan Flash, 433 nm ± 10 nm Tecan 200Pro) and the fluorescence emission spectra 460-580 nm was recorded (in 5 nm or 2 nm steps for Varioskan Flash and Tecan 200Pro, respectively). For FRET ratio determination, after background subtraction, emission ratios of mCit (525 ± 12 nm Varioskan Flash, 530 ± 20 nm Tecan 200Pro) and mCFP (475 ± 12 nm Varioskan Flash, 480 ± 20 nm Tecan 200Pro) were calculated. In samples with bosutinib, bosutinib autofluorescence was subtracted by calculating the difference in fluorescence intensities between the cell lysates of bosutinib-treated cells expressing and not expressing Src-FRET biosensor. Further, mCit fluorescence (λ_{ex} 500 ± 9 nm, λ_{em} 530 ± 20 nm) was determined for control of biosensor variants expression in individual cell lines.

For FRET analysis in cell lysates after stretch, the fluorescence spectra could not be reliably recorded due to low amount of sample material and, as a consequence, low fluorescence intensities in the spectral mode measurements. Instead, FRET was measured as a ratio of FRET fluorescence intensity (λ_{ex} 433 ± 9 nm, λ_{em} 530 ± 20 nm) and the fluorescence intensity of mCFP (λ_{ex} 433 ± 9 nm, λ_{em} 480 ± 20 nm). In order to compare in-between independent experiments, the data were normalized with respect to the FRET ratio of unstretched cells which was arbitrary set to 1. In all FRET steady-state measurements, the gating for each experimental cohort was set to same value, which was computed from sample with the highest fluorescence intensity within the cohort.

Fluorescence Microscopy

Cell Immunostaining and Confocal Microscopy

Cells were seeded on coverslips coated with 10 μg/ml fibronectin (Invitrogen) and grown for 12 - 24 h. Subsequently, the cells were fixed in 4% paraformaldehyde, permeabilized using 0.3% Triton X-100, washed with PBS and blocked in 3% bovine serum albumin in PBS. Samples were then sequentially incubated with primary antibodies for 3 h, secondary antibodies for 1 h, phalloidin for 15 min,

and extensively washed with PBS between each step. The slides were mounted in Mowiol 4–88 (Millipore) containing 1,4-diazobicyclo-[2.2.2]-octane (Sigma). The secondary antibodies were anti-rabbit-IgG Alexa Fluor 546 and anti-mouse-IgG Alexa Fluor 633 (Invitrogen). F-actin was probed with phalloidin conjugated with Alexa Fluor 405 (Dyomics) or Alexa Fluor 555 (Life Technologies). Images were acquired using Leica TCS SP8 microscope system equipped with a Leica 63×/ 1.45 NA oil objective.

FRET Sensitized Emission Analysis

U2OS cells were transiently co-transfected with the Src-FRET(T) biosensor and mCherry-FAT or mCherry-vinculin using polyethylenimine transfection agents (Sigma). Prior imaging the cells were trypsinized and allowed to attach on 35 mm dishes with glass bottom coated with fibronectin (MatTek, MA) and imaged in a window 30-60 min after seeding. FRET experiments were performed using Nikon Ti-E microscope with Nikon CFI HP Apo TIRF 100x Oil, NA 1.49. The microscope was equipped with two cameras, Andor iXon Ultra DU897 (Andor Technologies, UK) for acquisition of images excited with 445 nm and 488 nm laser beams, and Hamamatsu ORCA 4.0 V2 (Hamamatsu Photonics, Japan) for acquisition of images excited with 561 nm laser beam. Image splitter (DualView DV2, Photometrics, AZ) with filter cube splitting the beam at 505 nm was inserted in the light path preceding the Andor camera. Obtained dual images were processed using ImageJ. FRET, corrected for spectral bleed-throughs and normalized to donor fluorescence, was calculated as nF/I_{CFP} according to (Xia and Liu, 2001) in ImageJ using PixFRET plug-in (Feige et al., 2005).

Fluorescence Recovery after Photobleaching (FRAP)

U2OS cells were transiently co-transfected with the Src-FRET(T) biosensor and mCherry-vinculin using polyethylenimine transfection agents (Sigma). Prior imaging the cells were trypsinized and allowed to attach for 4 hours on 35 mm dishes with glass bottom coated with fibronectin (MatTek, MA). FRAP experiments were performed using Leica SP8 confocal microscope with a 63×/1.45 NA oil immersion objective. White light laser set to 512 nm was used to excite mCit and to 584 nm to excite mCherry. The focal adhesion was detected according to mCherry-FAT signal and in the selected focal adhesion the mCit signal was bleached using a high energy beam. The image acquisition started 5 s before bleaching and continued for approximately 30 s (one frame every 1.301 s). The recovery curves of the bleached regions were calculated from extracted image series using LAS X software (Leica), and the recovery halftime values were calculated from the FRAP curves by nonlinear regression analysis as described in (Tolde et al., 2012).

QUANTIFICATION AND STATISTICAL ANALYSIS

All the data were presented as mean ± standard deviation (SD) or ± standard error (SEM) from at least three independent experiments. The significance of differences was analyzed with one-way ANOVA followed by Tukey's honest significant difference test using GraphPad Prism software (version 6.07, GraphPad Software Inc.). Statistical significance was defined as $p < 0.05$. FRAP data fitting was performed in Excel using Solver add-in (Microsoft). FRET was calculated as nF/I_{CFP} according to (Xia and Liu, 2001) in ImageJ using PixFRET plug-in (Feige et al., 2005).